ACS APPLIED MATERIALS & INTERFACES

www.acsami.org Research Article

Ultraviolet Exciton-Polariton Light-Emitting Diode in a ZnO Microwire Homojunction

Maosheng Liu, Mingming Jiang,* Qinzhi Zhao, Kai Tang, Shulin Sha, Binghui Li, Caixia Kan, and Da Ning Shi*

Cite This: ACS Appl. Mater. Interfaces 2023, 15, 13258−13269

Read Online

ACCESS | Metrics & More | Article Recommendations | Supporting Information

ABSTRACT: Low-dimensional ZnO, possessing well-defined side facets and optical gain properties, has emerged as a promising material to develop ultraviolet coherent light sources. However, the realization of electrically driven ZnO homojunction luminescence and laser devices is still a challenge due to the absence of a reliable p-type ZnO. Herein, the sample of p-type ZnO microwires doped by Sb (ZnO:Sb MWs) was synthesized individually. Subsequently, the p-type conductivity was examined using a single-MW field-effect transistor. Upon optical pumping, a ZnO:Sb MW showing a regular hexagonal cross-section and smooth sidewall facets can feature as an optical microcavity, which is evidenced by the achievement of whispering-gallery-mode lasing. By combining an n-type ZnO layer, a single ZnO:Sb MW homojunction light-emitting diode (LED), which exhibited a typical ultraviolet emission at a wavelength of 379.0 nm and a line-width of approximately 23.5 nm, was constructed. We further illustrated that strong exciton-photon coupling can occur in the as-constructed p-ZnO:Sb MW/n-ZnO homojunction LED by researching spatially resolved electroluminescence spectra, contributing to the exciton-polariton effect. Particularly, varying the cross-sectional dimensions of ZnO:Sb wires can further modulate the exciton-photon coupling strengths. We anticipate that the results can provide an effective exemplification to realize reliable p-type ZnO and tremendously promote the development of low-dimensional ZnO homojunction optoelectronic devices.

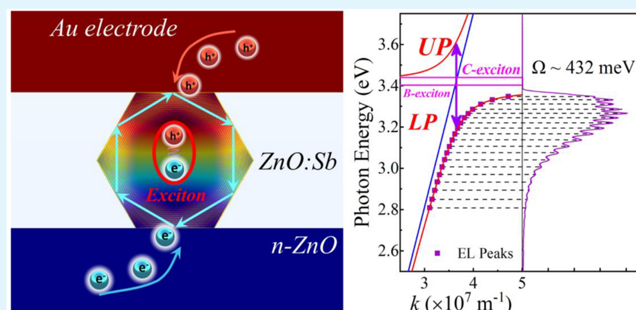

KEYWORDS: *exciton-polariton, electrically driven, p-ZnO:Sb MWs, homojunction LED, WGM microcavity*

Downloaded via CHANGCHUN INST OMP on May 13, 2024 at 07:48:50 (UTC).
See https://pubs.acs.org/sharingguidelines for options on how to legitimately share published articles.

INTRODUCTION

Ultraviolet (UV) light sources, including light-emitting diodes (LEDs) and laser diodes (LDs), are of fundamental interest in a wide range of applications, e.g., bioanalytical, material processing, water purification, plant lighting, free-space optical communication, disinfection, and medical diagnostics.[1−5] Traditionally, UV light sources are mainly based on semiconductors with bandgap energies larger than 3.0 eV, such as SnO_2, ZnO, GaN, etc.[6−10] Among these, GaN-based materials are the most commercially used in the design and fabrication of UV LEDs and LDs due to the successful manufacture of light emitters with reasonable p-type conductive characteristics.[6,8,11−13] However, when working at high current injection levels, these optoelectronic devices would suffer a severe reduction of the internal quantum efficiency (IQE), the so-called efficiency droop.[14,15] That is caused by high in-plane strain, strong piezoelectric polarization fields, inevitable carrier leakage, and so forth.[14,16,17] Moreover, the realistic applications of GaN-based micro/nanoscale LEDs and LDs are hindered by the synthesis of high-quality nano/micromaterials, which are commonly based on time-consuming and expensive single-crystal synthesis techniques; high vacuum and high temperature are necessary for these synthesis techniques.[18−20] Briefly speaking, the achievement of low-cost and high-quality single-crystalline nano/micromaterials, especially for commercial manufacture of low-dimensional UV LEDs and LDs, still remains a long-term and arduous task.

As a widely investigated semiconductor, ZnO possesses a wide bandgap of 3.37 eV and an exciton binding energy of 60 meV, which make it highly favorable for developing UV LEDs and LDs with high efficiency.[7,12,21] Meanwhile, the structural and material superiorities at the micro-nanoscale can offer desired candidates for developing a low-dimensional optoelectronic device.[12,22,23] However, ZnO optoelectronic devices are still limited by the unacceptable crystalline and electrical properties of p-type ZnO.[24,25] In recent years, group I elements (Li, Na, K)[26−28] and group V elements (including N, P, As,

Received: November 3, 2022
Accepted: February 21, 2023
Published: March 3, 2023

© 2023 American Chemical Society

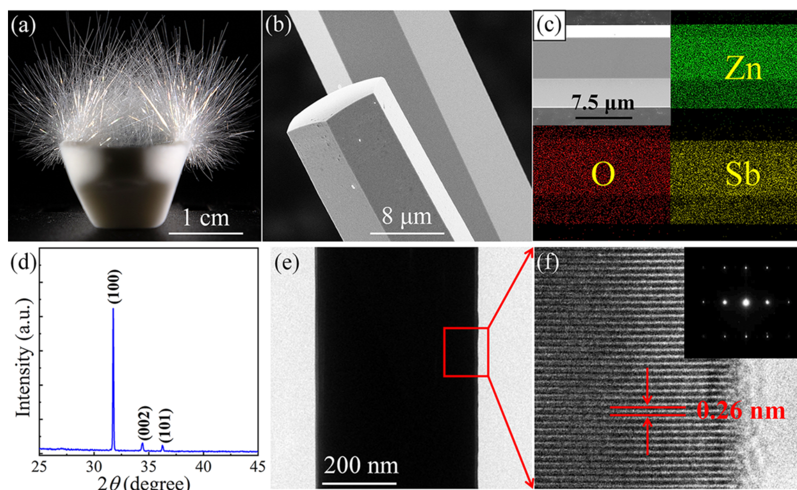

Figure 1. Characterization of CVD-prepared ZnO:Sb MWs. (a) Optical photograph of the as-synthesized ZnO:Sb MWs, which can be obtained around the Si substrate individually. (b) SEM image of ZnO:Sb MWs with regular hexagon-shaped cross section. (c) EDS images of a typical ZnO:Sb MW. (d) XRD pattern of CVD-synthesized ZnO:Sb wires. (e) A low-magnification TEM image of a ZnO:Sb wire, with its cross-sectional size of about 500 nm. (f) Focused at the selected region in (e), a high-resolution TEM image of a ZnO:Sb wire shows that the interplanar distance is derived to about 0.260 nm. (inset) The corresponding SAED analysis of the MW.

and Sb)[22,29−31] have been extensively employed as dopants for synthesizing p-type ZnO. But the doping of group V elements in ZnO severely suffered a poor p-type doping efficiency due to the formation of compensating interstitial.[26−28] Similarly, the applications for P(As)-doped ZnO are also severely limited by their low solubility and self-compensation effect.[32] N-Doped ZnO and the corresponding homojunction LEDs have been reported by some groups. However, due to the high defect densities and unsatisfactory solubility of N acceptors, the emissions of these devices mainly located in the blue band rather than the UV band.[22,24,33] It is remarkable that Sb has been comprehensively used to synthesize p-type ZnO due to the similar ionic radii of Sb^{3+} (0.076 nm) and Zn^{2+} (0.074 nm) for the formation of Sb_{Zn}-$2V_{Zn}$ complex acceptor theoretically and experimentally.[31,34] And many researchers have made considerable progress on the advances of preparing Sb-doped ZnO and the related homojunction optoelectronic devices by using molecular beam epitaxy (MBE), aqueous solution deposition, chemical vapor deposition (CVD), pulsed laser deposition (PLD), and so on.[32,35] Nevertheless, these LEDs emit blue/purple light with wavelength longer than that of ZnO band-edge emission in the luminescence spectrum, and the corresponding applications are still limited by low brightness and unsatisfactory output power. Therefore, it remains a tough challenge to synthesize genuine p-type ZnO with a high-quality single-crystalline nature, high stability, and reproducibility.

Utilizing Sb_2O_3 powder as an efficient impurity, p-type Sb-incorporated ZnO microwires (ZnO:Sb MWs) were successfully synthesized using a facile chemical vapor deposition (CVD) in this study. The CVD-prepared ZnO:Sb samples possessed highly crystalline qualities and superior lasing gain properties, which were confirmed by the achievement of whispering gallery mode (WGM) lasing upon optical excitation via a femtosecond pulsed laser. The p-type conductive characteristics of individual ZnO:Sb MWs were experimentally checked using single-MW-based field-effect transistors (FETs). To further distinguish the p-type conductive nature, a homostructure containing n-type ZnO film and p-type ZnO:Sb MW was constructed, yielding a standard rectifying property. The device exhibited a typical UV electroluminescence (EL) peaking at 379.0 nm and a line width of approximately 23.5 nm, giving rise to excitonic-related recombination in the ZnO:Sb wire channel. By exploiting the spatially resolved electroluminescence (EL) spectra, a series of interference peaks with ever-increasing mode spacing toward the low-energy shoulder can be ascribed to an exciton-polariton effect. The dependence of photon-exciton coupling strength via varied vacuum Rabi splitting on the cross-sectional sizes of the used ZnO:Sb MWs was also observed. Our work not only represents an advancement toward the synthesis of reliable p-type ZnO micro/nanocrystal materials but also provides a novel design to construct low-dimensional ZnO homojunction optoelectronic devices, such as relatively pure UV LEDs, electrically driven exciton-polariton LEDs, ultralow threshold LDs, and so on.

EXPERIMENTAL SECTION

Synthesis of Individual ZnO:Sb MWs. In a typical synthesis of individual ZnO:Sb MWs, a facile CVD method was conducted. Highly purified Sb_2O_3 powder (∼99.99%) as an incorporating source was mixed into the precursor materials, which contain currently used ZnO (99.99% in purity) and graphite (C, 99.99% in purity) powders. All the reagents were commercially purchased from ZhongNuo Advanced Material (Beijing) Technology Co., Limited. A precursor mixture of raw and preprocessed materials, which was typically made of 1.35 g of ZnO, 0.15 g of Sb_2O_3, and 1.5 g of C powders, was mixed thoroughly in an agate mortar. The precursor mixture was transferred to a curved alumina boat with a size of 5 cm (length) × 3.5 cm (width) × 2.5 cm (depth). A catalyst-free Si chip with a size of 3.5 cm (length) × 2.5 cm (width) was placed on the top of the alumina boat to collect the as-synthesized products. The vertical distance between the source materials and Si chip is about 2.0 cm. The alumina boat was positioned at the heating zone of the horizontal tube electric furnace. Before heating, a constant flow of Ar gas with 250 sccm was injected into the furnace to make the quartz tube experience an oxygen-deficient environment. The electric furnace was then raised up to about 1100 °C as soon as possible. Subsequently, a flow of protecting gas (Ar) with a flow rate of 120 sccm was kept constant during the growth process. After maintaining the growth temperature (∼1100 °C) for about 1 h, a flow of oxygen (O_2, 10 sccm), working as a growth gas, was employed in the furnace chamber. Afterward, the

https://doi.org/10.1021/acsami.2c19806
ACS Appl. Mater. Interfaces 2023, 15, 13258−13269

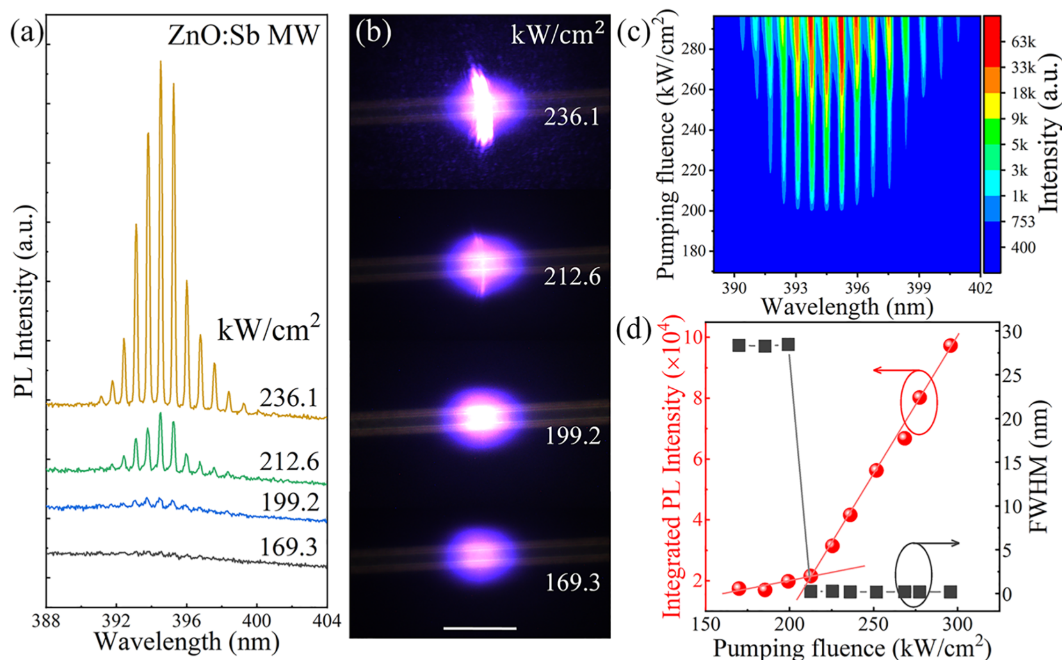

Figure 2. Lasing characterization of a single hexagonal ZnO:Sb MW. (a) PL spectra of a single ZnO:Sb MW under different pumping fluence (169.3−236.1 kW/cm^2) show broad spontaneous emission spectra below the threshold of 212.6 kW/cm^2 and sharp lasing peaks above the threshold. (b) Optical microscopic PL images of the as-prepared ZnO:Sb MW under different pumping fluence in the range of 169.3−236.1 kW/cm^2 (scale bar: 20 μm). (c) Contour plot of the PL emission under different pumping fluence for the hexagonal ZnO:Sb MW. (d) Variations of the integrated PL intensity and fwhm vs the pumping fluence for the hexagonal ZnO:Sb MW.

furnace chamber was cooled down to room temperature naturally after about 30 min of the growth process at the constant growth temperature. Individual ZnO:Sb wires can be collected on the Si chip. By varying the weight ratio of ZnO/Sb_2O_3/C, the Sb-doping concentration in the MWs can be varied. Figure S1 shows the energy-dispersive X-ray spectroscopy (EDS) mapping and the corresponding energy spectra of two samples with ZnO/Sb_2O_3/C = 9:1:10 and ZnO/Sb_2O_3/C = 5:1:6. Optical photograph of the as-prepared ZnO:Sb MWs is shown in Figure 1a. Shown in the image, ultralong ZnO/Sb MWs can reach up to about 2.5 cm, and the diameters vary in the range of 0.5−50 μm.

Device Fabrication. Employing n-type ZnO film as an electron transporting layer, a homojunction light-emitting device was constituted by combining an individual ZnO:Sb MW. The device fabrication process is listed as follows. First, a ZnO film (thickness: 200 nm) was grown on sapphire using a molecular beam epitaxy (MBE) system equipped with oxford radio frequency (RF) atom sources. Second, a layer of MgO film (thickness: 100 nm) was deposited on one of the sides for ZnO film using electron beam evaporation; then, two MgO films (thickness: 8 μm) employed as the bilateral insulating media were further deposited on the ZnO film. The gap distance between the bilateral MgO layers was controlled to about 50 μm. Third, a Au layer (~120 nm) serving as an n-type electrode was prepared on the other side of the ZnO film, while Au film (~50 nm in thickness) was evaporated on the predeposited MgO film utilizing electron beam heating evaporation. Fourth, an individual ZnO:Sb MW was mechanically transferred to a place on the ZnO film, with one segment of the wire placed on the Au nanofilm, which was prepared on the MgO layer. Fifth, a Au electrode was subsequently prepared on the segment of ZnO:Sb MW, which was placed on the Au film. Finally, a piece of quartz plate was placed at the top of ZnO:Sb MW. A moderate compressive stress was perpendicularly applied onto the quartz plate, guaranteeing a good contact between ZnO:Sb MW and ZnO film. The fabrication process and optical photograph of the as-designed p-ZnO:Sb MW/n-ZnO homojunction LED can be seen in Figures S2 and S3, respectively.

Material Characterizations. The sample shape, surface morphology, and microstructure of CVD-synthesized ZnO:Sb wires were measured by utilizing field-emission scanning electron microscopy (SEM) (TESCAN LAYRA3 GM) equipped with EDS under a HV of 20 kV. The samples were also analyzed using field-emission transmission electron microscopy (TEM) (Tecnai G2 F20) operated at 160 kV. The sample of ZnO:Sb wires was investigated by X-ray diffraction (XRD) via a Panalytical Empyrean diffractometer (λ = 1.5406 Å) to determine the material and phase compositions. Optical properties of as-grown ZnO:Sb samples and ZnO film were carried out utilizing a 325 nm He−Cd laser as the the excitation light source. The achievement of ZnO:Sb MW lasing was carried out via a pulse laser system, which contained a 355 nm femtosecond laser (pulse duration of 150 fs, repetition rate of 1000 Hz) and an optical multichannel analyzer (Princeton, Acton SP2500i). The electrical properties of the fabricated ZnO:Sb MW FETs and p-ZnO:Sb MW/n-ZnO homojunction LEDs were characterized using a Keysight semiconductor device analyzer (Keithley, B1500A). Electroluminescence (EL) characterizations of the as-fabricated LEDs were tested using a testing system, which was made of a microscope (Olympus), a spectrometer (LabRAM-UV Jobin-Yvon), and a high-sensitivity charge-coupled device (CCD), while the emission graphs were obtained using a CCD camera.

RESULTS AND DISCUSSION

The product of individual ZnO:Sb MWs was successfully acquired by using a carbothermal reduction method via a self-catalyzed approach. Figure 1a shows the optical photograph of CVD-synthesized ZnO:Sb MWs. One can see that the ZnO:Sb MWs can reach exceptional lengths at the centimeter level, demonstrating relatively long ZnO-based MWs by comparing with previous works.[36,37] The shape profiles, elemental constituents, and structure of CVD-synthesized ZnO:Sb MWs were characterized. As shown in Figure 1b, ZnO:Sb MWs exhibit regular hexagonal cross-sections, smooth boundaries, and sidewall facets. Another ZnO:Sb MW was performed to examine the internal and elementary constituents using EDS elemental mapping. As shown in Figure 1c, the

https://doi.org/10.1021/acsami.2c19806
ACS Appl. Mater. Interfaces 2023, 15, 13258−13269

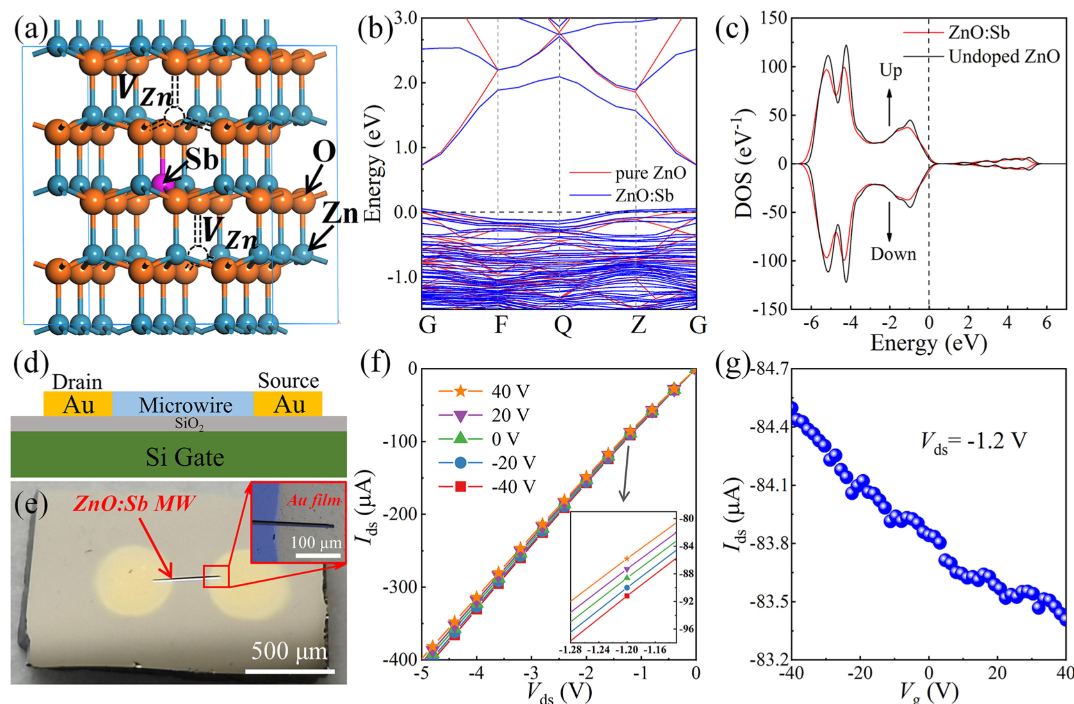

Figure 3. Characterizing the p-type conductivity of individual ZnO:Sb wires. (a) Schematic structure of the Zn, O, and Sb atom in the Sb-doped ZnO lattice. A complex structure of the Sb_{Zn}-$2V_{Zn}$ contains a Sb substitution on a Zn site, which is surrounded by two Zn vacancies. (b) Band structure of undoped ZnO and Sb-doped ZnO. The Fermi energy level of the Sb-doped ZnO goes into the valence band. (c) The state density distribution of undoped ZnO and Sb-doped ZnO. (d) Schematic diagram of the as-designed single ZnO:Sb wire-based FET. (e) Optical photograph of the fabricated FET, with an enlarged view of ZnO:Sb MW placed on the Au film illustrated in the inset. (f) The plot of I_{ds} as a function of V_{ds} of the ZnO:Sb MW-based FET, which was measured at different V_g. (inset) Enlarged view of the I_{ds}-V_{ds} curves at ca. −1.2 V. I_{ds}-V_g curve at V_{ds} = −1.2 V. (g) The variation of I_{ds}, which is dependent on the V_g.

mapped Zn, Sb, and O species distribute homogeneously throughout the entire wire. The XRD pattern illustration in Figure 1d exhibits that all the strongest peaks match well with the standard data (JCPDS No. 36-1451). The intense diffraction peaks positioned at around 31.75°, 34.45°, and 36.24° can be assigned to (100), (002), and (101) planes, respectively.[39] We further implemented the TEM measurement to determine the crystallographic structure of a ZnO:Sb wire with its cross-sectional size at a submicron scale. A low-magnification TEM observation shown in Figure 1e demonstrates that the as-synthesized ZnO:Sb wire exhibits a regular profile of straight and smooth boundaries and uniform widths. Focused at a selected region, a high-resolution TEM image illustrates that the interplanar distance, which is parallel to the crystallographic planes, is measured to about 0.26 nm (see Figure 1f). The inset selected-area electron diffraction (SAED) analysis of the wire exhibits a single set of electron diffraction spots, suggesting the single-crystalline property of ZnO:Sb wires.[38,39]

It was previously reported that ZnO nano- and microstructures with a regular hexagonal cross section can be utilized as optical cavity resonators, supporting WGM lasing.[40−42] The well-defined geometric construction and single-crystalline quality can render the as-synthesized ZnO:Sb samples as efficient lighting sources and a laser medium for stimulated radiation.[42,43] A single ZnO:Sb MW with hexagonal cross section was excited optically at room temperature by using a femtosecond-amplified laser (∼355 nm) as the excitation source. Figure 2a shows representative photoluminescence (PL) spectra via different excitation densities. At low excitation fluence of ∼169.3 kW/cm^2, a broad emission band peaking at 393.5 nm with a full-width at half-maximum (fwhm) of 18.3 nm can be observed. As the excitation intensity increases up to 199.2 kW/cm^2, several resonant peaks appear in the PL spectrum. As we further increased the excitation intensities, the number of sharp peaks and their intensities increased rapidly, while the intensity of the broad spontaneous emission peak (nonlasing) remained almost constant, suggesting WGM lasing operation.[21] Taking a PL spectrum at an excitation power density of 236.1 kW/cm^2 for an example, the PL spectrum is dominated by a series of sharp peaks, while the spontaneous radiation was distinctly suppressed. The mode spacing of ∼$\Delta\lambda$ between two neighboring peaks is nearly constant, indicating the same waveguide origin of the sharp emission modes.[42] The average fwhm is derived to about 0.19 nm. According to the WGM cavity formula $N = 3\sqrt{3}Dn/2\lambda - 6\tan^{-1}(n\sqrt{3n^2 - 4})/\pi$, the computed lasing wavelengths match well with the PL spectrum. Conclusively, the CVD-synthesized ZnO:Sb wires with regular hexagonal cross section can be utilized to construct WGM microlaser devices.[42,44] Besides, the lasing quality factor Q of the ZnO:Sb MW microlaser is calculated to be 2079 according to the equation $Q = \lambda/\delta\lambda$, in which λ is the emission wavelength.[42,44]

Optical microscopic PL images obtained at different excitation densities are illustrated in Figure 2b. Especially, the lasing light can escape primarily from the sharp edges as the excitation densities go beyond the laser threshold. The PL results show the transformation from broad spontaneous emission to stimulated radiation.[44] Figure 2c illustrates the two-dimensional (2D) pseudocolor plot for the PL spectra versus different pumping fluence for the ZnO:Sb MW. The

https://doi.org/10.1021/acsami.2c19806
ACS Appl. Mater. Interfaces 2023, 15, 13258−13269

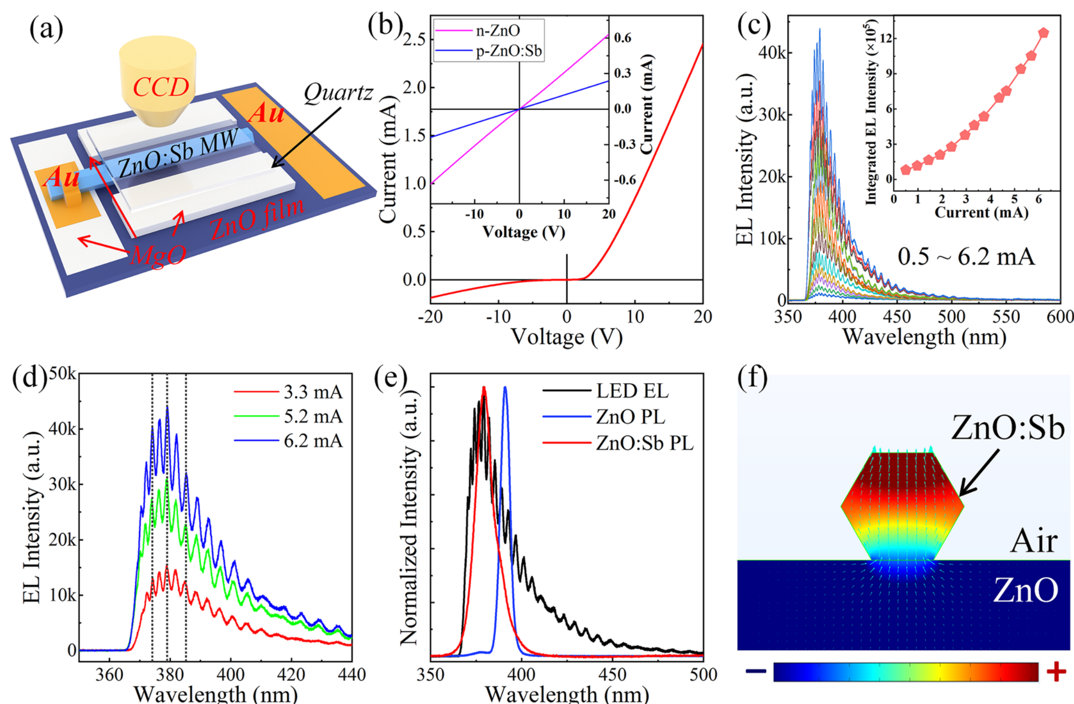

Figure 4. Device characterization of as-constructed p-ZnO:Sb MW/n-ZnO homojunction LED. (a) Schematic architecture of the homojunction emission device. (b) $I-V$ characteristic curve of as-constructed p-ZnO:Sb MW/n-ZnO homostructure device. (inset) $I-V$ characteristic curves of an individual ZnO:Sb MW and ZnO film, respectively. (c) EL spectra of as-constructed p-ZnO:Sb MW/n-ZnO homojunction emission device by varying the forward current in the range of 0.5−6.2 mA. (inset) Variation of the integrated EL intensity under different injection currents. (d) Several EL spectra selected from (c) when the injection current were 3.3, 5.2, and 6.2 mA, respectively. (e) Normalized intensities of the EL spectrum of the LED, the PL spectra of ZnO film, and ZnO:Sb MW, respectively. (f) The calculated electrostatic potential distribution of as-constructed p-ZnO:Sb/n-ZnO homojunction LED.

variations of integrated PL intensity and the fwhm versus the pumping fluence are shown in Figure 2d. The fwhm decreases from 18.4 nm for spontaneous emission to 0.19 nm for stimulated radiation, indicating the onset of lasing action with a threshold of $P_{th} \approx 212.6$ kW/cm^2. The results described above confirmed the formation of the natural WGM microresonator due to the high crystallinity for the hexagon-shaped ZnO:Sb MWs.[40,42,44] Therefore, the CVD-synthesized ZnO:Sb MWs with high crystallinity and low defect densities can supply highly reliable platforms to develop droop-free LEDs and LDs.[7,45]

To investigate the influence of Sb-dopant on the electronic transport properties of CVD-synthesized ZnO products, theoretical analysis and calculation for large-size mismatched impurities was carried out by using first-principle calculations. As previously analyzed, isolated Sb may form donor (Sb_{Zn}), deep acceptor (Sb_O), or antimony interstitial (Sb_i). Thus, Sb-related defect complexes could be generated in the Sb-doped ZnO samples. However, none of these could result in the p-type conductive characteristic.[46−48] As a low-energy defect with shallow acceptor levels, the formed Sb_{Zn}-$2V_{Zn}$ complex could be considered as the origin for the p-type conductive characteristic of ZnO. In the complex, an Sb atom occupies the Zn site, further inducing two Zn vacancies spontaneously.[46,47,49] To illustrate the p-type conductive properties for the Sb-doped ZnO, a theoretical analysis based on first-principles calculations was carried out using Materials Studio. A schematic of pure ZnO structure with Zn and O atoms in the lattice is shown in Figure S4. By contrast, the schematic lattice structure for Sb-doped ZnO with an Sb_{Zn}-$2V_{Zn}$ complex acceptor is shown in Figure 3a.[46] The detailed parameters and calculation method have been provided in the Supporting Information. Figure 3b shows the obtained energy-band structure distributions of undoped ZnO (red solid line) and Sb-doped ZnO (blue solid line), in which the energy zero point is the Fermi level. One can see that the Fermi level of Sb-doped ZnO goes into the valence band, showing the p-type conductive characteristic by comparing with the undoped ZnO.[50] In addition, the total state density distribution of the undoped ZnO (black solid line) and Sb-doped ZnO (red solid line) is shown in Figure 3c, respectively. As presented in the figure, the partial state density of holes occupied the valence band, which is consistent with the band structure analysis. Therefore, the p-type conductive characteristic for the proposed model with a Sb_{Zn}-$2V_{Zn}$ complex acceptor can be created in theory.[50]

Experimentally, to examine the electronic transport properties of CVD-grown ZnO:Sb products, a single MW-based FET was constructed by combining SiO_2/Si substrate and a single ZnO:Sb wire.[38,51] A schematic illustration of an as-designed single ZnO:Sb wire-based FET device is shown in Figure 3d. The optical photograph of the fabricated FET (Au film working as electrodes) is shown in Figure 3e. The inset shows an enlarged view of the ZnO:Sb MW, which is placed on the Au film electrode. Electrical characterizations of the fabricated ZnO:Sb MW FET device were performed using a Keysight semiconductor device analyzer. Varying the back-gate voltages (V_g), Figure 3f depicts the variations of the source-drain current (I_{ds}) as a function of source-drain voltage (V_{ds}). The enlarged view of the I_{ds}-V_{ds} curves measured at around V_{ds} = 1.2 V is further shown in the inset of Figure 3f. Additionally, the variation of source-drain current (I_{ds}) versus V_g was further

https://doi.org/10.1021/acsami.2c19806
ACS Appl. Mater. Interfaces 2023, 15, 13258−13269

determined, as illustrated in Figure 3g. Thus, the typical p-type conductive characteristics of an individual ZnO:Sb wire could be confirmed by the decreases (increases) of the conductance when the V_g increase is positive (negative).[38,51]

Electrical properties of as-synthesized ZnO:Sb MW, including conductivity, mobility, and carrier concentration, can be calculated by the following equations. First, according to the equation

$$R = \rho\frac{l}{S} = \frac{l}{\sigma S} \quad (1)$$

where R is the resistance, ρ is the resistivity, σ is the conductivity, l is the length of MWs, and S is the cross-sectional area of MWs. The carrier mobility (μ) of MWs can be estimated according to the following formula.[52]

$$g_m = \rho\frac{l}{A} = \frac{l}{\sigma A} \quad (2)$$

In the formula, g_m and C are defined as channel conductance of MW-based FET and capacitance of the MWs, respectively. And C can be obtained from[53]

$$C = \frac{2\pi\varepsilon_0\varepsilon_{SiO_2}l}{\cosh^{-1}(1 + 2h/d)} \quad (3)$$

where ε_0 is the vacuum dielectric constant, ε_{SiO2} is the relative dielectric constant of SiO_2 (3.9), and h and d are the thickness of the SiO_2 (300 nm) and the diameter of the ZnO:Sb MWs, respectively, while the carrier concentration n was then calculated using the following formula[54]

$$\rho = \frac{l}{\sigma} = \frac{l}{nq\mu} \quad (4)$$

in which q is the elementary charge. Accordingly, the conductivity, mobility, and carrier concentration of the selected ZnO:Sb MW are determined to be 0.087 S/cm, 11.32 $cm^2\ V^{-1}\ s^{-1}$, and $4.35 \times 10^{17}\ cm^{-3}$, respectively. Making a better comparison, an FET device based on an undoped ZnO MW has been constructed (the corresponding results can be seen in Figure S6). The ZnO MW shows a typical n-type conduction nature with a carrier concentration and mobility of $9.52 \times 10^{17}\ cm^{-3}$ and 19.06 $cm^2\ V^{-1}\ s^{-1}$, respectively. It indicates that Sb doping can be used to achieve the transform of the conduction type from n- to p-type. Thus, the two critical factors, low defect densities (which have been proved by the achieved WGM lasing), and outstanding electrical properties of CVD-prepared ZnO:Sb MWs are verified. These features confirmed that an individual ZnO:Sb MW can work as an efficient droop-free luminescent material, which is desired in the design and fabrication of high-efficiency LEDs.[7,45]

A homojunction optoelectronic device made of an n-type ZnO film and a single p-type ZnO:Sb MW was constructed. The device structure of the p-ZnO:Sb MW/n-ZnO homojunction is schematically shown in Figure 4a, in which Au films work as the electrodes. The optical photograph of a real device is shown in Figure S3. The 100 nm MgO layer is used as an insulating medium between ZnO film and the Au electrode, which has been evaporated on the ZnO:Sb MW. A Keysight semiconductor analyzer (B1500A) was employed to characterize the electrical properties for the homojuction LED. The $I-V$ curve plotted in Figure 4b shows a typical diode-like rectification characteristic. An individual ZnO:Sb MW and the used ZnO film were also tested by using Au electrodes to reveal their electronic transport properties. The $I-V$ curves are shown in the inset of Figure 4b. From the figure, one can conclude that the good ohmic contacts between Au and the ZnO film (ZnO:Sb MW) were formed, indicating that the standard rectifying behavior resulted from the high-quality homojunction created between the p-ZnO:Sb MW and n-ZnO film. The turn-on voltage is derived to be 2.6 V.[12,37] That is also evidence of the p-type conductive characteristic for the ZnO:Sb samples, which were originated from the Sb_{Zn}-$2V_{Zn}$ complex acceptors.

EL characterizations of our fabricated p-ZnO:Sb MW/n-ZnO homojunction LED device were performed at room temperature. When driven electrically, the emitted photons were obtained using a charge-coupled device (CCD) spectrometer (PIXIS). EL spectra versus injection current varying from 0.5 to 6.2 mA is plotted in Figure 4c. Shown in the graph, prominent UV spectra with a main wavelength of about 379.0 nm (fwhm ≈ 23.5 nm) can be observed. The peak wavelength is nearly constant as the injection current increased, yielding a stable UV emission. Meanwhile, the EL light-emitting images (illustrated in Figure S7) were recorded via the CCD camera, showing that emission regions distribute all over the MW. Shown in the inset of Figure 4c, an approximatively linear character is illustrated by the variations of the integrated emission intensities versus the operating current. The linear behavior implies that the UV EL is successfully dominated through the radiative recombination occurring in the ZnO:Sb MW active medium.[55,56] When fixed at 3.3, 5.2, and 6.2 mA, respectively, the plotted EL spectra illustration in Figure 4d can be utilized to confirm the stability of our homojunction LEDs. Besides, there are no observable variations of the wavelengths for the resonance peaks and spectral profiles of EL spectra, illustrating an insensitivity to the quantum confined stark effect (QCSE).[55,56] This indicates that the depletion region and radiative recombination of the as-constructed p-ZnO:Sb MW/n-ZnO homojunction are unaltered, even measured at high current densities.

To study the EL mechanism, photoluminescence (PL) measurements of an individual ZnO:Sb MW and ZnO film were measured. Given for a comparison, Figure 4e presents the normalized PL spectra of ZnO:Sb MW and ZnO film and a normalized EL spectrum of the fabricated LED. Shown in the figure, the PL spectrum of ZnO film (the solid blue line) is dominated by a narrow UV emission peaking at 391.1 nm (the line width of ~7.0 nm), while the PL spectrum of ZnO:Sb MW (solid violet line) exhibits a dominant UV emission centered at 379.6 nm with an fwhm of about 14 nm. The EL profile (the solid black line) illustrates a typical UV emission peaking at around 379.0 nm, which matched well with the PL peak of the CVD-synthesized ZnO:Sb MWs. One can conclude that the EL emissions of the fabricated p-ZnO:Sb MW/n-ZnO homojunction LED mainly result from the radiative recombination that happened in the p-ZnO:Sb MW channel; the light-emitting regions that happened in the ZnO film or in the ZnO:Sb/ZnO interface can be suppressed effectively.[12,43,58]

Furthermore, the finite-difference time-domain (FDTD) method was used to figure up the electrostatic potential field distribution of our fabricated p-ZnO:Sb MW/n-ZnO homojunction LED numerically via a computational fluid dynamics model. According to the real device, a three-dimensional model was constructed. The cross-sectional profile of the LED model is further shown in Figure S2. The materials' parameters of used ZnO:Sb MW and ZnO film are enumerated in Table 1.

https://doi.org/10.1021/acsami.2c19806
ACS Appl. Mater. Interfaces 2023, 15, 13258−13269

Table 1. Electrical Transport Properties of the Selected ZnO:Ga MWs

Parameters	ZnO:Sb MW	n-ZnO film
Mobility ($cm^2\ V^{-1}\ s^{-1}$)	11.32	10.79
Concentration (cm^{-3})	4.35×10^{17}	3.62×10^{19}

In the calculation, a forward bias fixed at ~10 V was applied at designated boundaries to feature as the reference for the simulation of the electrical-potential distribution. As the calculation was accomplished, the electrical potential functions for electrostatic fields were solved utilizing Maxwell's equations, electrostatics, quantum mechanics, and solid mechanics. Finally, the electrical-potential distribution of our designed p-ZnO:Sb MW/n-ZnO homojunction LED device under a forward bias could be computed and acquired via postprocessing. From the simulated result in Figure 4f, one can see that the electroneutral region is principally distributed in the ZnO:Sb MW channel. Thereby, the radiative recombination mainly occurred in the ZnO:Sb MW. Essentially, the confinement behavior was analyzed and can be attributed to the carrier concentration discrepancy between the ZnO film (3.62×10^{19} cm^{-3}) and ZnO:Sb MW (4.35×10^{17} cm^{-3}). The much higher carrier concentration of ZnO film would cause a massive injection of electrons into the ZnO:Sb MW when the device was operated under a forward bias.[7,57] During the occurrence of recombination for electrons and holes, a mass of excitons can be formed due to the Coulomb interaction. Then strong coupling between excitons and cavity photons, which, being confined in the optical microcavity, would occur.[37,58] In this case, the as-synthesized individual ZnO:Sb MWs can function as an active and luminescence region, while the ZnO film was rolled as a current spreading layer to provide uniform electron injection, thus realizing the effective carrier injection and electron−hole recombination in the single wire active media.[7,45] The obtained EL emission featuring in the UV band can be interpreted as the typical near band edge (NBE) emission of ZnO:Sb MW in our fabricated homojunction LEDs. The results indicate the successful confinement of carriers for the ZnO:Sb MW with high crystallinity and preferable carrier concentration. The as-synthesized individual ZnO:Sb MW can not only work as hole-injecting sources but also serve as a luminescence region and high-quality optical resonant cavity. By a careful modulation of the electrical characteristics of the as-synthesized ZnO:Sb samples and ZnO layer, the as-constructed p-ZnO:Sb MW/n-ZnO homojunction can highly concentrate the injected charge carriers in the ZnO:Sb MW active region.[7,45] Conclusively, the as-constructed p-ZnO:Sb MW/n-ZnO homojunction is expected to enable the realization of low-dimensional high-brightness and droop-free UV light sources, which are suitable for operation at high temperatures and high current densities.

It is evidently noted that multiple emission peaks can be clearly seen in the plotted EL spectra, and the corresponding mode spacings are becoming smaller when the photon energy approaches the exciton resonance, as the as-synthesized single ZnO:Sb MW with hexagonal cross-section can naturally feature as a typical WGM cavity. Thus, the optical resonance can be created through total internal reflection at the cavity

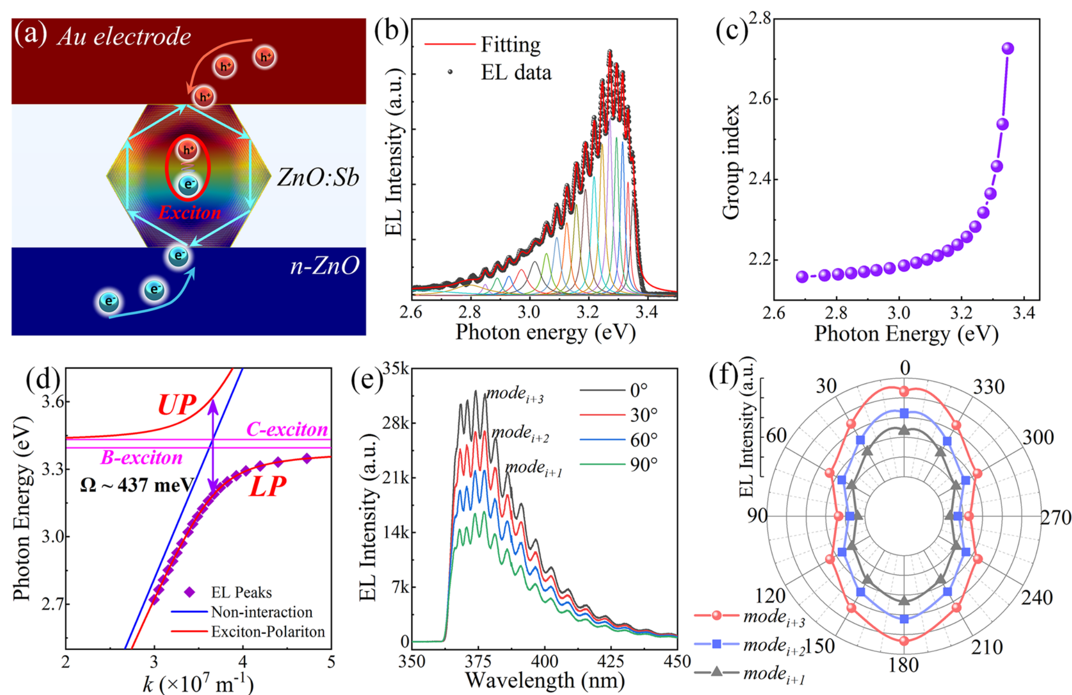

Figure 5. Exciton-polariton emission features of as-constructed p-ZnO:Sb MW/n-ZnO homojunction LED. (a) The emergence of exciton-polariton EL characteristics realized in the as-constructed single ZnO:Sb wire homojunction LED, which is resulted from strong coupling between the exciton and the photonic mode of a hexagonal MW microresonator. (b) EL spectrum via multiple interference peaks, which is fitted by a Lorentzian (The forward injection current ≈ 6.2 mA). (c) The dependence of group refractive index as a function of the photon energy of the as-constructed homojunction LED. (d) The energy-wavevector dispersion curves, in which the Rabi splitting energy is extracted to about 437 meV. (e) The angle-resolved EL spectra by varying degree of detection polarization. A series of oscillation peaks with corresponding resonance modes denoted as "$mode_{i+1}$", "$mode_{i+2}$", and "$mode_{i+3}$" is marked. (f) Polar plots of the measured EL intensity as a function of the emission polarization angle.

https://doi.org/10.1021/acsami.2c19806
ACS Appl. Mater. Interfaces 2023, 15, 13258−13269

boundary. Consider that the energies of optical modes are positioned relatively in UV wavelengths, which are close the ZnO:Sb excitons. It is expected that excitons can strongly couple with cavity photons in the ZnO:Sb MW channel.[37,43] To understand the relative pure UV emission spectra of the as-constructed p-ZnO:Sb MW/n-ZnO homojunction emission devices properly, exciton-polariton effect should be discussed in detail. Figure 5a exhibits the schematic illustration of a coupling system between exciton and WGM modes of the generated photons, which are confined in the naturally formed hexagonal microcavity under electrical excitation. As we stated above, the electrons and holes can be injected into the ZnO:Sb wire channel simultaneously. Due to the Coulomb interaction, the excitons can be generated and confined in the ZnO:Sb MW microresonator, while the as-synthesized ZnO:Sb MWs illustrate well-defined geometric structures and highly crystallized quality. The observed oscillation modes, which have been resolved from the recorded EL spectra, cannot be understood with the aid of a traditional photonic model. Thus, a strong coupling interaction can happen in the as-constructed p-ZnO:Sb MW/n-ZnO homojunction LEDs as well as the generation of exciton-polariton quasi-particles. The achieved multiple resonance peaks on the EL spectra would be attributed to the polariton emission.[43,59]

More interestingly, as illustrated in Figure 5b, a series of sharp subpeaks can be well-fitted by Lorentzian line shapes. The modes of exciton-polaritons can be assigned to the multiple peaks, and the mode spacing decreased from 43.3 to 16.8 meV as the photon energy increased in the scope of 2.69–3.35 eV. These uneven mode spacings are unambiguous evidence of strong exciton-photon coupling that occurred in the ZnO:Sb MW, suggesting the observable dispersion and increase of group index.[37,59,60] The Q-factor of our fabricated p-ZnO:Sb MW/n-ZnO homojunction LED is extracted to about 270, which is much lower than that of the identical ZnO:Sb MW ($Q \approx 2079$) upon the excitation of femtosecond-pulsed laser. Generally, the WGM microcavity supports polarization modes in hexagonal ZnO microcrystals.[37,43,59] And the formula for WGM-type resonance energy is as follows.[59,61]

$$E = \frac{2hc}{3\sqrt{3}\,\tilde{n}(\omega)d}\left[N + \frac{6}{\pi}\arctan\left(\frac{1}{\tilde{n}(\omega)}\right)\sqrt{3\tilde{n}(\omega)^2 - 4}\right] \tag{5}$$

In this formula, E, h, and c are the photon energy of the resonance peaks, Planck constant, and velocity of light, respectively. The d and $\tilde{n}(\omega)$ are the diameter and refractive index of the ZnO:Sb MW, respectively. The expression of the dispersion relation of the refractive index $\tilde{n}(\omega)$ for ZnO can be supplied as follows

$$\tilde{n}(\omega) = \tilde{\varepsilon}(\omega)^2 = \varepsilon_b(\omega) + \sum_{i=A,B,C} g_i \frac{{\omega_{iL}}^2 - {\omega_{iT}}^2}{{\omega_{iT}}^2 - \omega^2 - i\omega\Gamma_i} \tag{6}$$

where $\varepsilon_b(\omega)$ is the background permittivity determined by the frequency, g_i is a dimensionless parameter that relates to the oscillator strength; three excitons caused by the split valence bands were defined as $i = A, B, C$, respectively. ω_{iL}, ω_{iT}, and Γ_i are the longitudinal and transverse resonance frequencies of excitons and the damping term, respectively.[40,61]

In previous works, $\varepsilon_b(\omega)$ is equal to ε_0. From Equation 6, one can see that the refractive index will deviate rapidly when the frequency ω approaches ω_{iT}. And the refractive index cannot be well-fitted by the lower (or higher) extracted value g_i if the $\varepsilon_b(\omega)$ is overestimated (underestimated), further causing an inaccuracy of the Rabi splitting energy.[62] To overcome this issue, an iterative approach was employed to extract the dispersion relation around the resonance frequency. The WGM resonance frequency (ω_N or λ_N) of the oscillation peaks with assigned mode number N can be easily obtained in the hexagonal ZnO:Sb MWs. The wavelength-dependent group index $n_g(\lambda_N)$ at each WGM resonance wavelength λ_N can be calculated by the mode spacing $\lambda_{N+1} - \lambda_N = \Delta\lambda_N$, which can be easily obtained from the EL spectra. The corresponding equations are as follows.[62]

$$\lambda_{N+1} - \lambda_N = \Delta\lambda_N = \frac{{\lambda_N}^2}{L'\left[n(\lambda_N) - \lambda_N \frac{dn}{d\lambda_N}\right]} \tag{7}$$

$$n(\lambda_{N+1}) = n(\lambda_N) + \Delta\lambda_N \frac{dn}{d\lambda_N} \tag{8}$$

In Equation 7, L' is the length of the optical path for WGM modes in the ZnO:Sb MW, which can be easily calculated using $L' = 3\sqrt{3}R$ (R: the radius of ZnO:Sb MW). Here $n_g(\lambda_N) = n(\lambda_N) - \lambda_N\frac{dn}{d\lambda_N}$ is the group index. The slope of refractive index $\frac{dn}{d\lambda_N}$ at λ_N can be obtained when the refractive index $n(\lambda_N)$ at the Nth resonance λ_N is determined (see Equation 7). Then, λ_{N+1} can be calculated by utilizing Equation 8. As previously reported, low light–matter coupling strength can barely affect the group refractive index. Hence, the refractive index $n(\lambda_N)$ at $\lambda_N \approx hc/2.69$ eV, at which the oscillation peak with lowest energy located, was chosen to be the initial value. The dispersion of $n(\lambda)$ can be computed iteratively by using the values of $n(\lambda_N)$ and $\frac{dn}{d\lambda_N}$ obtained from mode spacing in EL spectrum near λ_N.

Figure 5c shows the variations of group refractive index n_g versus photon energy. Clearly, the n_g value hardly changes at all (~2.15) in the lower-energy side, and then it grows much faster as the photon energy approaches ZnO:Sb excitons. For example, the n_g can distinctly increase up to 2.77 at peak energy of the plotted EL spectra (~3.31 eV). In the higher photon energy regime, the n_g is much larger than that of the bulk ZnO materials. This unnatural increase of group index suggests that a strong exciton-photon coupling interaction would occur in the p-ZnO:Sb MW/n-ZnO homojunction LED, further confirming the exciton-polariton quasi-particle features.[59,62] The exciton-polariton dispersion in k space was calculated, and the corresponding energy-wavevector dispersion curves in the x-y plane (in the cross section of ZnO:Sb MW) of as-constructed p-ZnO:Sb MW/n-ZnO homojunction LED are illustrated in Figure 5d according to Equation 5. The upper polariton (UP) and lower polariton (LP) branches were formed as a result of coherent oscillation between the cavity photon state and the exciton state.[59,60,62] In the exciton-photon strong coupling model, these optical modes are primarily situated on the LP of exciton-polariton dispersion curves, which are largely due to the severe damping influence of the UP. Nonresonant high-energy excitations will generate reservoir excitons, and the dynamics of reservoir excitons can be used to explain the damping of the UP.[60] Besides, in the hexagonal ZnO:Sb MW microcavity, the band edge absorption,

https://doi.org/10.1021/acsami.2c19806
ACS Appl. Mater. Interfaces 2023, 15, 13258−13269

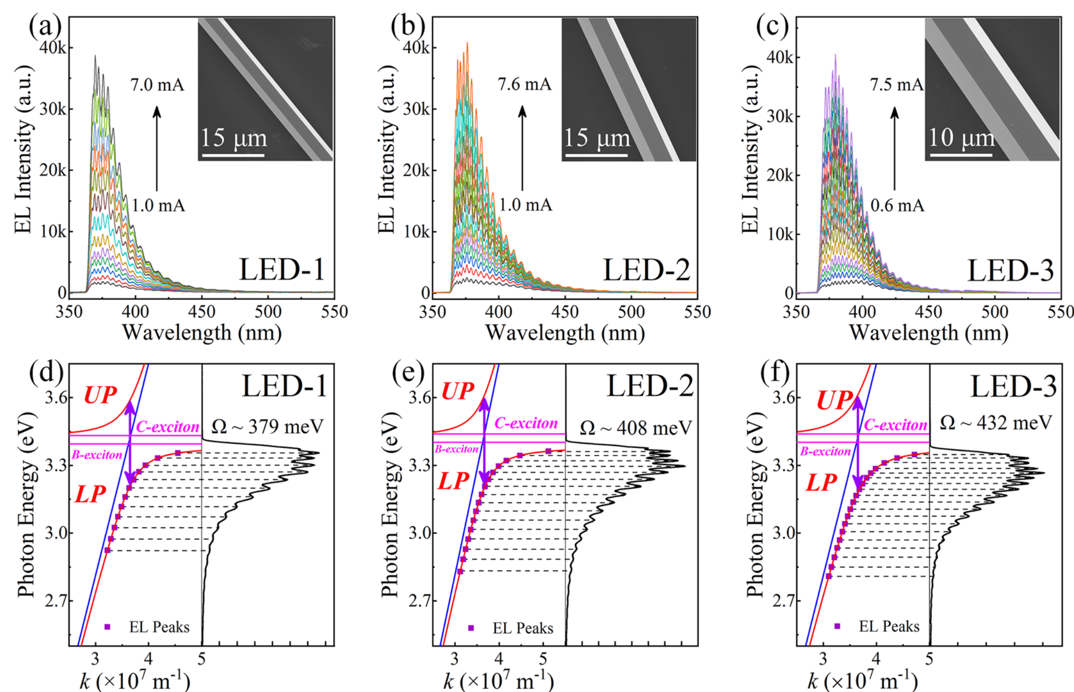

Figure 6. Size-dependent exciton−polariton EL characteristics of the as-constructed p-ZnO:Sb MW/n-ZnO homojunction LEDs. (a) The plotted EL spectra of LED-1, with the hexagonal diameter of ZnO:Sb MW that is derived to about 4.8 μm. (inset) SEM image of ZnO:Sb MW. (b) EL spectra of LED-2. (inset) SEM image of the used ZnO:Sb MW, and the hexagonal diameter is evaluated to about 7.2 μm. (c) EL spectra of LED-3. (inset) SEM image of the used ZnO:Sb MW, and the hexagonal diameter is evaluated to about 9.8 μm. The energy-wavevector dispersion curves and EL spectra of the as-constructed LEDs (d) for LED-1, in which the Rabi splitting energy is extracted to about 379 meV, (e) for LED-2, the Rabi splitting energy ~408 meV, (f) for LED-3, the Rabi splitting energy ~432 meV.

waveguide loss, and thermal relaxation of the medium will cause a decay of polaritons in the UP toward the LP branches.[37,43] Conclusively, a rapid nonradiative extinction of the UP will occur as the excited UP is scattered to the exciton reservoir. The reserved excitons will scatter into LP states through phonon emission.[60] This phenomenon is responsible for the novel multipeak emission with controllable periods in the UV wavelengths for the as-constructed p-ZnO:Sb MW/n-ZnO homojunction LEDs. The coupling strength between exciton and the confined optical mode is also illustrated in Figure 5d through the minimum energy difference between UP and LP branches. That is, the Rabi splitting energy ≈ Ω as indicated by the violet arrow in Figure 5d is derived to about 437 meV.

It was previously reported that the emitted photons of the hexagonal MW-based LED mainly distribute at the sharp edges, and the emission intensity distribution is periodical with a period angle.[12,37,43] Thus, by using the PIXIS CCD detection system, far-field angle-resolved EL signals were collected and analyzed to investigate the exciton-polariton characteristics of the homojunction LED. In the angle-resolved EL measurement, the slit of monochromator is perpendicular to the axial direction of the ZnO:Sb MW, and the device was rotated along the axial direction of the ZnO:Sb MW. As illustrated in Figure 5e, there is an observable variation in the EL intensities but little changes of the mode spacing when the collection angle varies from 0° to 90° at an injection current of 6.2 mA. Besides, three resonance peaks denoted as "$mode_{i+1}$", "$mode_{i+2}$", and "$mode_{i+3}$" were selected to reveal the exciton-polariton features.

The degree of polarization (DOP) of the selected modes in the range of 0° to 360° was further demonstrated in Figure 5f. A distinct periodic change can be clearly seen when the detection angle increased. That can be attributed to the separation of perpendicular electric field ($E_\perp$) from parallel electric field ($E_\parallel$), which will occur when the detecting angle is changed.[43,59] Consequently, a dominated $E_\parallel$ component can be seen in the polarization of the light-emission modes. This phenomenon further indicates the strong exciton−photon coupling interaction achieved in the microcavities of hexagonal ZnO:Sb MWs.[37,59] Distinctly, these experimental results provide a new exemplification for the achievement of high coupling strengths, further promoting the design and fabrication of electrically driven polariton devices, e.g., coherence light sources, slow light, polariton lasers, and nonlinear optics.

As mentioned above, the hexagonal structure of the as-synthesized ZnO:Sb wires can perfectly confine the light waves, leading to the formation of WGM resonance. Given that, the influence of ZnO:Sb wires with different cross-sectional diameters on the exciton-polariton EL characteristics of the as-constructed p-ZnO:Sb MW/n-ZnO homojunction LEDs was researched. Individual ZnO:Sb MWs with identical lengths but different cross-sectional diameter d were selected, which were named Sample-1 ($d \approx 4.8$ μm), Sample-2 ($d \approx 7.2$ μm), and Sample-3 ($d \approx 9.8$ μm), respectively. Accordingly, the selected wires were employed to construct homojunction LEDs by combining an n-type ZnO layer, and these were denoted as LED-1, LED-2, and LED-3, respectively. Figure 6a−c illustrates the EL spectra of the as-constructed LEDs with similar injection current range. As illustrated in these figures, all the EL profiles are mainly positioned in the range of 360−425 nm. SEM images of the used ZnO:Sb wires are illustrated in the inset of Figure 6a−c. With increasing the cross-sectional

https://doi.org/10.1021/acsami.2c19806
ACS Appl. Mater. Interfaces 2023, 15, 13258−13269

sizes of the used individual ZnO:Sb MWs, the spectral profiles exhibit an observable broadening. Besides, one can see that the dominant EL peak wavelengths of LED-2 and LED-3 show observable redshifts of 6.8 and 9.8 nm when compared to that of the LED-1, respectively. This phenomenon indicates that increasing the cross-sectional diameter of ZnO:Sb MWs could result in enhanced polariton relaxation before releasing their extra energy as photons escaped from the confinement of ZnO:Sb MW microcavities.

The Lorentzian fitting results of the sharp peaks for the EL spectra of LED-1 to LED-3 were shown in Figure S8. It can be clearly seen that the resonance peaks for LED-2 and LED-3 are much denser than that of LED-1, indicating an increasing resonance strength and decreasing mode spacing as the cross-sectional diameter increased.[43] It further suggests that the stronger light−matter coupling strength can occur in the as-constructed homojunction LEDs with increasing the cross-sectional diameters of used ZnO:Sb MWs. The larger dimensions of as-prepared ZnO:Sb MWs can contribute to the stronger confinement in the *x*-*y* plane; these are distributed in the hexagon-shaped cross section. Sequentially, the exciton-polariton dispersion in the $\vec{k}$ spaces of LED-1, LED-2, and LED-3 was also calculated. The energy-wavevector dispersion curves and corresponding EL spectra are plotted in Figure 6d,e, respectively. According to Equation 5, the increasing Rabi splitting energy for LED-1 ($\Omega_{LED\text{-}1} \approx 379$ meV), LED-2 ($\Omega_{LED\text{-}2} \approx 408$ meV), and LED-3 ($\Omega_{LED\text{-}3} \approx 432$ meV) can be obtained, indicating the stronger light−matter coupling interaction in the ZnO:Sb MW with larger cross-sectional diameter.

■ CONCLUSIONS

To summarize, we have proposed an achievable approach to prepare reliable p-type ZnO wires and further enable the realization of electrically driven UV EL emissions based on an as-constructed p-ZnO:Sb MW/n-ZnO homojunction. The constructed homojunction exhibits excellent diode characteristics and can emit UV emission peaking at 379.0 nm with a line width of about 23.5 nm, indicating an effective injection of carrier and excitonic-type recombination in the used ZnO:Sb MW active media. More importantly, electrically driven exciton-polariton LEDs were realized by using the carefully designed p-ZnO:Sb MW/n-ZnO homojunction structure. The Rabi splitting energies, which reveal the exciton−photon coupling strength, can be controlled by varying the spatial dimensions of the as-synthesized ZnO:Sb wires. The results reported in this study are not only an advancement for fabricating reliable p-type ZnO microcrystals with the aid of Sb complex incorporation but also a remarkable step for the potential applications of a ZnO homojuncion optoelectronic device. We also expect that this work will become a motivation for further experimental results about the doping mechanisms for the achievement of p-type metal oxide wide bandgap semiconductor materials, such as SnO_2 and Ga_2O_3, which sheds light on the design of low-dimensional homojunction optoelectronic devices in the solar-blind UV spectral region.

■ ASSOCIATED CONTENT

Supporting Information

The Supporting Information is available free of charge at https://pubs.acs.org/doi/10.1021/acsami.2c19806.

EDS mapping results and their energy spectra of CVD-synthesized ZnO:Sb samples via different Sb-doping concentration; The fabrication procedure of as-designed single ZnO:Sb MW homojunction LED device; Optical photograph of a real homojunction LED; Theoretical calculation and analysis using first-principles; FET result based on an individual undoped ZnO MW; Optical micrographs of the fabricated LED when measured at different injection currents; the fitted EL spectra via multiple interference peaks of as-fabricated LEDs by using Lorentzian line shapes (PDF)

■ AUTHOR INFORMATION

Corresponding Authors

Mingming Jiang − *College of Physics, MIIT Key Laboratory of Aerospace Information Materials and Physics, Key Laboratory for Intelligent Nano Materials and Devices, Nanjing University of Aeronautics and Astronautics, Nanjing 211106, China*; orcid.org/0000-0003-1784-582X; Email: mmjiang@nuaa.edu.cn

Da Ning Shi − *College of Physics, MIIT Key Laboratory of Aerospace Information Materials and Physics, Key Laboratory for Intelligent Nano Materials and Devices, Nanjing University of Aeronautics and Astronautics, Nanjing 211106, China*; Email: shi@nuaa.edu.cn

Authors

Maosheng Liu − *College of Physics, MIIT Key Laboratory of Aerospace Information Materials and Physics, Key Laboratory for Intelligent Nano Materials and Devices, Nanjing University of Aeronautics and Astronautics, Nanjing 211106, China*

Qinzhi Zhao − *College of Physics, MIIT Key Laboratory of Aerospace Information Materials and Physics, Key Laboratory for Intelligent Nano Materials and Devices, Nanjing University of Aeronautics and Astronautics, Nanjing 211106, China*

Kai Tang − *College of Physics, MIIT Key Laboratory of Aerospace Information Materials and Physics, Key Laboratory for Intelligent Nano Materials and Devices, Nanjing University of Aeronautics and Astronautics, Nanjing 211106, China*

Shulin Sha − *College of Physics, MIIT Key Laboratory of Aerospace Information Materials and Physics, Key Laboratory for Intelligent Nano Materials and Devices, Nanjing University of Aeronautics and Astronautics, Nanjing 211106, China*

Binghui Li − *State Key Laboratory of Luminescence and Applications, Changchun Institute of Optics Fine Mechanics and Physics, Chinese Academy of Sciences, Changchun 130033, China*

Caixia Kan − *College of Physics, MIIT Key Laboratory of Aerospace Information Materials and Physics, Key Laboratory for Intelligent Nano Materials and Devices, Nanjing University of Aeronautics and Astronautics, Nanjing 211106, China*; orcid.org/0000-0003-3722-422X

Complete contact information is available at: https://pubs.acs.org/10.1021/acsami.2c19806

Author Contributions

Maosheng Liu: Conceptualization, Sample Preparation, Device Fabrication and Characterizations, Analysis, Writing- Original

draft preparation. Mingming Jiang: Methodology, Formal analysis, Data curation, Conceptualization, Funding acquisition, Writing-review and editing, Supervision. Qinzhi Zhao: Sample Preparation, Device Characterizations. Kai Tang: Device Characterization, Formal analysis, Data curation. Shulin Sha: Theoretical calculation and Analysis. Binghui Li: Sample Preparation, Analysis, Conceptualization. Caixia Kan: Funding acquisition, Supervision. Daning Shi: Conceptualization, Resources, Supervision, Funding acquisition, Writing-review and editing. All authors read and approved the final manuscript.

Notes

The authors declare no competing financial interest.

■ ACKNOWLEDGMENTS

This study was supported by the National Natural Science Foundation of China (Grant Nos. 11974182 and 11874220), the Fundamental Research Funds for the Central Universities (No. NC2022008), and Funding for Outstanding Doctoral Dissertation in NUAA (BCXJ22-14).

■ REFERENCES

(1) Wang, J.; Chen, H.; Zhao, Y.; Zhong, Z.; Tang, Y.; Liu, G.; Feng, X.; Xu, F.; Chen, X.; Cai, D.; Kang, J. Programmed Ultrafast Scan Welding of Cu Nanowire Networks with a Pulsed Ultraviolet Laser Beam for Transparent Conductive Electrodes and Flexible Circuits. *ACS Appl. Mater. Interfaces* **2020**, *12*, 35211−35221.

(2) Alwadai, N.; Ajia, I. A.; Janjua, B.; Flemban, T. H.; Mitra, S.; Wehbe, N.; Wei, N.; Lopatin, S.; Ooi, B. S.; Roqan, I. S. Catalyst-Free Vertical ZnO-Nanotube Array Grown on p-GaN for UV-Light-Emitting Devices. *ACS Appl. Mater. Interfaces* **2019**, *11*, 27989−27996.

(3) Liu, C.; Hu, Q.; Zhang, C.; Xia, C.; Yin, H.; Su, W.; Wang, X.; Xu, Y.; Zhang, Z. First Chinese Ultraviolet-Visible Hyperspectral Satellite Instrument Implicating Global Air Quality during the COVID-19 Pandemic in Early 2020. *Light: Sci. Appl.* **2022**, *11*, 28.

(4) Fang, M.-H.; Bao, Z.; Huang, W.-T.; Liu, R.-S. Evolutionary Generation of Phosphor Materials and Their Progress in future applications for Light-Emitting Diodes. *Chem. Rev.* **2022**, *122*, 11474−11513.

(5) Kneissl, M.; Seong, T.; Han, J.; Amano, H. The Emergence and Prospects of Deep-Ultraviolet Light-Emitting Diode Technologies. *Nat. Photonics* **2019**, *13*, 233−244.

(6) Ren, Z.; Yu, H.; Liu, Z.; Wang, D.; Xing, C.; Zhang, H.; Huang, C.; Long, S.; Sun, H. Band Engineering of III-Nitride-Based Deep-Ultraviolet Light-Emitting Diodes: A Review. *J. Phys. D: Appl. Phys.* **2020**, *53*, 073002.

(7) Nikoobakht, B.; Hansen, R. P.; Zong, Y.; Agrawal, A.; Shur, M.; Tersoff, J. High-Brightness Lasing at submicrometer enabled by droop-free fin light-emitting diodes (LEDs). *Sci. Adv.* **2020**, *6*, No. eaba4346.

(8) Chang, H.; Liu, Z.; Yang, S.; Gao, Y.; Shan, J.; Liu, B.; Sun, J.; Chen, Z.; Yan, J.; Liu, Z.; Wang, J.; Gao, P.; Li, J.; Liu, Z.; Wei, T. Graphene-Driving Strain Engineering to enable strain-free epitaxy of AlN Film for Deep Ultraviolet Light-Emitting Diode. *Light: Sci. Appl.* **2022**, *11*, 88.

(9) Huang, Y.; Li, Y.; Yao, B.; Ding, Z.; Deng, R.; Zhang, L.; Zhao, H. A Facile Route to Realize Ultraviolet Emission in a Nano-Engineered SnO_2-Based Light-Emitting Diode. *J. Phys. D: Appl. Phys.* **2015**, *48*, 465103.

(10) Li, J.; Gao, N.; Cai, D.; Lin, W.; Huang, K.; Li, S.; Kang, J. Multiple Fields Manipulation on Nitride Material Structures in Ultraviolet Light-Emitting Diodes. *Light: Sci. Appl.* **2021**, *10*, 129.

(11) Li, D.; Jiang, K.; Sun, X.; Guo, C. AlGaN Photonics: Recent Advances in Materials and Ultraviolet Devices. *Adv. Opt. Photon.* **2018**, *10*, 43−110.

(12) Zhou, X.; Jiang, M.; Xu, K.; Liu, M.; Sha, S.; Cao, S.; Kan, C.; Shi, D. N. Electrically Driven Single Microwire-Based Single-Mode Microlaser. *Light: Sci. Appl.* **2022**, *11*, 198.

(13) Zhu, H.; Shan, C.; Yao, B.; Li, B.; Zhang, J.; Zhang, Z.; Zhao, D.; Shen, D.; Fan, X.; Lu, Y.; Tang, Z. Ultralow-Threshold Laser Realized in Zinc Oxide. *Adv. Mater.* **2009**, *21*, 1613−1617.

(14) Iveland, J.; Martinelli, L.; Peretti, J.; Speck, J. S.; Weisbuch, C. Direct Measurement of Auger Electrons Emitted from a Semiconductor Light-Emitting Diode under Electrical Injection: Identification of the Dominant Mechanism for Efficiency Droop. *Phys. Rev. Lett.* **2013**, *110*, 177406.

(15) Auf der Maur, M.; Pecchia, A.; Penazzi, G.; Rodrigues, W.; Di Carlo, A. Efficiency Drop in green InGaN/GaN light emitting diodes: the role of Random Alloy Fluctuations. *Phys. Rev. Lett.* **2016**, *116*, 027401.

(16) Wang, D.; Wu, W.; Fang, S.; Kang, Y.; Wang, X.; Hu, W.; Yu, H.; Zhang, H.; Liu, X.; Luo, Y.; He, J.-H.; Fu, L.; Long, S.; Liu, S.; Sun, H. Observation of Polarity-Switchable Photoconductivity in III-Nitride/MoS_x Core-Shell Nanowires. *Light: Sci. Appl.* **2022**, *11*, 227.

(17) Yu, Y.; Wang, T.; Chen, X.; Zhang, L.; Wang, Y.; Niu, Y.; Yu, J.; Ma, H.; Li, X.; Liu, F.; Deng, G.; Shi, Z.; Zhang, B.; Wang, X.; Zhang, Y. Demonstration of Epitaxial Growth of strain-relaxed GaN films on graphene/SiC substrates for Long Wavelength Light-Emitting Diodes. *Light: Sci. Appl.* **2021**, *10*, 117.

(18) Ra, Y.-H.; Navamathavan, R.; Yoo, H.-I.; Lee, C.-R. Single Nanowire Light-Emitting Diodes Using Uniaxial and Coaxial InGaN/GaN Multiple Quantum Wells Synthesized by Metalorganic Chemical Vapor Deposition. *Nano Lett.* **2014**, *14*, 1537−1545.

(19) Ra, Y.-H.; Wang, R.; Woo, S. Y.; Djavid, M.; Sadaf, S. M.; Lee, J.; Botton, G. A.; Mi, Z. Full-Color Single Nanowire Pixels for Projection Displays. *Nano Lett.* **2016**, *16*, 4608−4615.

(20) Tchoe, Y.; Lee, C.-H.; Park, J. B.; Baek, H.; Chung, K.; Jo, J.; Kim, M.; Yi, G.-C. Microtube Light-Emitting Diode Arrays with Metal Cores. *ACS Nano* **2016**, *10*, 3114−3120.

(21) Xu, C.; Dai, J.; Zhu, G.; Zhu, G.; Lin, Y.; Li, J.; Shi, Z. Whispering-Gallery Mode Lasing in ZnO Microcavities. *Laser Photonics Rev.* **2014**, *8*, 469−494.

(22) Wei, Z. P.; Lu, Y. M.; Shen, D. Z.; Zhang, Z. Z.; Yao, B.; Li, B. H.; Zhang, J. Y.; Zhao, D. X.; Fan, X. W.; Tang, Z. K. Room Temperature p-n ZnO Blue-Violet Light-Emitting Diodes. *Appl. Phys. Lett.* **2007**, *90*, 042113.

(23) Yang, X.; Dong, L.; Shan, C.; Sun, J.; Zhang, N.; Wang, S.; Jiang, M.; Li, B.; Xie, X.; Shen, D. Piezophototronic-Effect-Enhanced Electrically Pumped Lasing. *Adv. Mater.* **2017**, *29*, 1602832.

(24) Chen, A.; Zhu, H.; Wu, Y.; Chen, M.; Zhu, Y.; Gui, X.; Tang, Z. Beryllium-Assisted p-Type Doping for ZnO Homojunction Light-Emitting Devices. *Adv. Funct. Mater.* **2016**, *26*, 3696−3702.

(25) Shi, L.; Wang, F.; Li, B.; Chen, X.; Yao, B.; Zhao, D.; Shen, D. A Highly Efficient UV Photodetector Based on a ZnO Microwire p-n Homojunction. *J. Mater. Chem. C* **2014**, *2*, 5005−5010.

(26) Chang, Y.-T.; Chen, J.-Y.; Yang, T.-P.; Huang, C.-W.; Chiu, C.-H.; Yeh, P.-H.; Wu, W.-W. Excellent Piezoelectric and Electrical Properties of Lithium-Doped ZnO Nanowires for Nanogenerator Applications. *Nano Energy* **2014**, *8*, 291−296.

(27) Qi, J.; Huang, J.; Paul, D.; Ren, J.; Chu, S.; Liu, J. Current Self-Complianced and Self-Rectifying Resistive Switching in Ag-Electroded Single Na-Doped ZnO Nanowires. *Nanoscale* **2013**, *5*, 2651−2654.

(28) Bai, J.; Xu, X.; Xu, L.; Cui, J.; Huang, D.; Chen, W.; Cheng, Y.; Shen, Y.; Wang, M. Potassium-Doped Zinc Oxide as Photocathode Material in Dye-Sensitized Solar Cells. *ChemSusChem* **2013**, *6*, 622−629.

(29) Mishra, M.; Sushama, S.; Pandey, S. K.; Chakrabarti, S. Phosphorus Doping of ZnO Using Spin-On Dopant Process: A Better Choice Than Costly and Destructive Ion-Implantation Technique. *J. Lumin.* **2021**, *233*, 117921.

(30) Cho, H. D.; Zakirov, A. S.; Yuldashev, S. U.; Ahn, C. W.; Yeo, Y. K.; Kang, Đ. W. Homojunction p-n Photodiodes Based on As-Doped Single ZnO Nanowire. *AIP Conf. Proc.* **2013**, *1566*, 51−52.

https://doi.org/10.1021/acsami.2c19806
ACS Appl. Mater. Interfaces 2023, 15, 13258−13269

(31) Baek, S.-D.; Biswas, P.; Kim, J.-W.; Kim, Y. C.; Lee, T. I.; Myoung, J.-M. Low-Temperature Facile Synthesis of Sb-Doped p-Type ZnO Nanodisks and Its Application in Homojunction Light-Emitting Diode. *ACS Appl. Mater. Interfaces* **2016**, *8*, 13018−13026.
(32) Fan, J.; Sreekanth, K.; Xie, Z.; Chang, S.; Rao, K. p-Type ZnO Materials: Theory, Growth, Properties and Devices. *Prog. Mater. Sci.* **2013**, *58*, 874−985.
(33) Su, M.; Zhang, T.; Su, J.; Wang, Z.; Hu, Y.; Gao, Y.; Gu, H.; Zhang, X. Homogeneous ZnO Nanowire Arrays p-n Junction for Blue Light-Emitting Diode Applications. *Opt. Express* **2019**, *27*, A1207−A1215.
(34) Lupan, O.; Chow, L.; Ono, L. K.; Cuenya, B. R.; Chai, G.; Khallaf, H.; Park, S.; Schulte, A. Synthesis and Characterization of Ag- or Sb-Doped ZnO Nanorods by a Facile Hydrothermal Route. *J. Phys. Chem. C* **2010**, *114*, 12401−12408.
(35) Chu, S.; Wang, G.; Zhou, W.; Lin, Y.; Chernyak, L.; Zhao, J.; Kong, J.; Li, L.; Ren, J.; Liu, J. Electrically Pumped Waveguide Lasing from ZnO Nanowires. *Nat. Nanotechnol.* **2011**, *6*, 506−510.
(36) Fan, H.; Xu, S.; Cao, X.; Liu, D.; Yin, Y.; Hao, H.; Wei, D.; Shen, Y. Ultra-Long Zn_2SnO_4-ZnO Microwires Based Gas Sensor for Hydrogen Detection. *Appl. Surf. Sci.* **2017**, *400*, 440−445.
(37) Jiang, M.; Wan, P.; Tang, K.; Liu, M.; Kan, C. An Electrically Driven Whispering Gallery Polariton Microlaser. *Nanoscale* **2021**, *13*, 5448−5459.
(38) Yuan, G.-D.; Zhang, W.-J.; Jie, J.-S.; Fan, X.; Tang, J.-X.; Shafiq, I.; Ye, Z.-Z.; Lee, C.-S.; Lee, S.-T. Tunable n-Type Conductivity and Transport Properties of Ga-Doped ZnO Nanowire Arrays. *Adv. Mater.* **2008**, *20*, 168−173.
(39) Jiang, M.; He, G.; Chen, H.; Zhang, Z.; Zheng, L.; Shan, C.; Shen, D.; Fang, X. Wavelength-Tunable Electroluminescent Light Sources from Individual Ga-Doped ZnO Microwires. *Small* **2017**, *13*, 1604034.
(40) Sun, L.; Chen, Z.; Ren, Q.; Yu, K.; Bai, L.; Zhou, W.; Xiong, H.; Zhu, Z. Q.; Shen, X. Direct Observation of Whispering Gallery Mode Polaritons and Their Dispersion in a ZnO Tapered Microcavity. *Phys. Rev. Lett.* **2008**, *100*, 156403.
(41) Miao, C.; Xu, H.; Jiang, M.; Liu, Y.; Wan, P.; Kan, C. High Performance Lasing in a Single ZnO Microwire Using Rh Nanocubes. *Opt. Express* **2020**, *28*, 20920−20929.
(42) Xu, C.; Qin, F.; Zhu, Q.; Lu, J.; Wang, Y.; Li, J.; Lin, Y.; Cui, Q.; Shi, Z.; Manohari, A. G. Plasmon-Enhanced ZnO Whispering-Gallery Mode Lasing. *Nano Res.* **2018**, *11*, 3050−3064.
(43) Kan, C.; Wu, Y.; Xu, J.; Wan, P.; Jiang, M. Plasmon-Enhanced Strong Exciton-Polariton Coupling in Single Microwire-Based Heterojunction Light-Emitting Diodes. *Opt. Express* **2021**, *29*, 1023−1036.
(44) Li, J.; Lin, Y.; Lu, J.; Xu, C.; Wang, Y.; Shi, Z.; Dai, J. Single Mode ZnO Whispering-Gallery Submicron Cavity and Graphene Improved Lasing Performance. *ACS Nano* **2015**, *9*, 6794−6800.
(45) Hansen, R. P.; Zong, Y.; Agrawal, A.; Garratt, E.; Beams, R.; Tersoff, J.; Shur, M.; Nikoobakht, B. Chip-Scale Droop-Free Fin Light-Emitting Diodes Using Facet-Selective Contacts. *ACS Appl. Mater. Interfaces* **2021**, *13*, 44663−44672.
(46) Limpijumnong, S.; Zhang, S. B.; Wei, S.-H.; Park, C. H. Doping by Large-Size-Mismatched Impurities: The Microscopic Origin of Arsenic- or Antimony-Doped p-Type Zinc Oxide. *Phys. Rev. Lett.* **2004**, *92*, 155504.
(47) Ren, X.; Zhang, X.; Liu, N.; Wen, L.; Ding, L.; Ma, Z.; Su, J.; Li, L.; Han, J.; Gao, Y. White Light-Emitting Diode from Sb-Doped p-ZnO Nanowire Arrays/n-GaN Film. *Adv. Funct. Mater.* **2015**, *25*, 2182−2188.
(48) Ke, X.; Shan, F.; Wang, G.; Liu, C.; Fu, D. Structural and Raman Analysis of Antimony-Implanted ZnMnO Films. *Plasma Sci. Technol.* **2010**, *12*, 92.
(49) Guo, W.; Allenic, A.; Chen, Y. B.; Pan, X. Q.; Che, Y.; Hu, Z. D.; Liu, B. Microstructure and Properties of Epitaxial Antimony-Doped p-Type ZnO Films Fabricated by Pulsed Laser Deposition. *Appl. Phys. Lett.* **2007**, *90*, 242108.
(50) Hou, Q.; Sha, S. Effect of Biaxial Strain on the p-Type of Conductive Properties of (S, Se, Te) and 2N Co-Doped ZnO. *Mater. Today Commun.* **2020**, *24*, 101063.
(51) Wan, P.; Jiang, M.; Xu, T.; Liu, Y.; Kan, C. High-Mobility Induced High-Performance Self-Powered Ultraviolet Photodetector Based on Single ZnO Microwire/PEDOT:PSS Heterojunction via Slight Ga-Doping. *J. Mater. Sci. Technol.* **2021**, *93*, 33−40.
(52) Cui, Q.; Hu, Y.; Zhou, C.; Teng, F.; Huang, J.; Zhugayevych, A.; Tretiak, S.; Nguyen, T.-Q.; Bazan, G. C. Single Crystal Microwires of p-DTS$(FBTTh_2)_2$ and Their Use in the Fabrication of Field-Effect Transistors and Photodetectors. *Adv. Funct. Mater.* **2018**, *28*, 1702073.
(53) Wunnicke, O. Gate Capacitance of Back-Gated Nanowire Field-Effect Transistors. *Appl. Phys. Lett.* **2006**, *89*, 083102.
(54) Yuan, G. D.; Ng, T. W.; Zhou, Y. B.; Wang, F.; Zhang, W. J.; Tang, Y. B.; Wang, H. B.; Luo, L. B.; Wang, P. F.; Bello, I.; Lee, C. S.; Lee, S. T. p-Type Conductivity in Silicon Nanowires Induced by Heterojunction Interface Charge Transfer. *Appl. Phys. Lett.* **2010**, *97*, 153126.
(55) Li, H.; Khoury, M.; Bonef, B.; Alhassan, A. I.; Mughal, A. J.; Azimah, E.; Samsudin, M. E.; De Mierry, P.; Nakamura, S.; Speck, J. S.; DenBaars, S. P. Efficient Semipolar (11−22) 550 nm Yellow/Green InGaN Light-Emitting Diodes on Low Defect Density (11−22) GaN/Sapphire Templates. *ACS Appl. Mater. Interfaces* **2017**, *9*, 36417−36422.
(56) Liu, M.; Jiang, M.; Liu, Y.; Tang, K.; Shi, D. N.; Kan, C. Wavelength-Tunable Green Light Sources Based on ZnO:Ga Nanowire/p-InGaN Heterojunctions. *ACS Appl. Nano Mater.* **2021**, *4*, 11168−11179.
(57) Wang, D.; Liu, M.; Shang, S.; Wan, P.; Shi, D.; Kan, C.; Li, B.; Jiang, M. An Individual ZnO Microwire Homojunction LED with Ultraviolet Electroluminescence Spectrally Purified Using Pt Nanoparticles Cladding. *Opt. Laser Technol.* **2023**, *160*, 109052.
(58) Jiang, M.; Mao, W.; Zhou, X.; Kan, C.; Shi, D. Wavelength-Tunable Waveguide Emissions from Electrically Driven Single ZnO/ZnO:Ga Superlattice Microwires. *ACS Appl. Mater. Interfaces* **2019**, *11*, 11800−11811.
(59) van Vugt, L. K.; Rühle, S.; Ravindran, P.; Gerritsen, H. C.; Kuipers, L.; Vanmaekelbergh, D. Exciton Polaritons Confined in a ZnO Nanowire Cavity. *Phys. Rev. Lett.* **2006**, *97*, 147401.
(60) Du, W.; Zhang, S.; Shi, J.; Chen, J.; Wu, Z.; Mi, Y.; Liu, Z.; Li, Y.; Sui, X.; Wang, R.; Qiu, X.; Wu, T.; Xiao, Y.; Zhang, Q.; Liu, X. Strong Exciton-Photon Coupling and Lasing Behavior in All-Inorganic $CsPbBr_3$ Micro/nanowire Fabry-Perot Cavity. *ACS Photonics* **2018**, *5*, 2051−2059.
(61) Vanmaekelbergh, D.; van Vugt, L. K. ZnO Nanowire Lasers. *Nanoscale* **2011**, *3*, 2783−2800.
(62) Wu, S.-C.; Zhuang, G.-Y.; Chang, Y.-C.; Hsu, H.-C. Determination of Dispersion Relation and Optical Parameters Induced by Exciton-Polariton Effect in Whispering-Gallery Microcavities Using Photoluminescence Spectroscopy. *ACS Photonics* **2021**, *8*, 1413−1420.